3BP2-deficient mice are osteoporotic with impaired osteoblast and osteoclast functions

Noam Levaot,[1] Paul D. Simoncic,[1] Ioannis D. Dimitriou,[1] Andrew Scotter,[1] Jose La Rose,[1] Adeline H.M. Ng,[2] Thomas L. Willett,[2] Chiachien J. Wang,[3] Salima Janmohamed,[1] Marc Grynpas,[2] Ernst Reichenberger,[3] and Robert Rottapel[1,4]

[1]Campbell Family Cancer Research Institute, Ontario Cancer Institute, Princess Margaret Hospital, University Health Network, Department of Medicine, University of Toronto, Toronto, Ontario, Canada. [2]Samuel Lunenfeld Research Institute, Mount Sinai Hospital, University of Toronto, Toronto, Canada. [3]Department of Oral Rehabilitation, Biomaterials and Skeletal Development, Center for Restorative Medicine and Skeletal Development, University of Connecticut Health Center, Farmington, Connecticut, USA. [4]St. Michael's Hospital, Department of Medicine, Toronto, Canada.

A fine balance between bone resorption by osteoclasts and bone formation by osteoblasts maintains bone homeostasis. In patients with cherubism, gain-of-function mutations in 3BP2, which is encoded by SH3-domain binding protein 2 (*SH3BP2*), cause cystic lesions with activated osteoclasts that lead to craniofacial abnormalities. However, little is known about the function of wild-type 3BP2 in regulating bone homeostasis. Here we have shown that 3BP2 is required for the normal function of both osteoblasts and osteoclasts. Initial analysis showed that *Sh3bp2*$^{-/-}$mice developed osteoporosis as a result of reduced bone formation despite the fact that bone resorption was impaired. We demonstrated using reciprocal bone marrow chimeras, a cell-intrinsic defect of the osteoblast and osteoclast compartments in vivo. Further, *Sh3bp2*$^{-/-}$ osteoblasts failed to mature and form mineralized nodules in vitro, while *Sh3bp2*$^{-/-}$ osteoclasts spread poorly and were unable to effectively degrade dentine matrix in vitro. Finally, we showed that 3BP2 was required for Abl activation in osteoblasts and Src activation in osteoclasts, and demonstrated that the in vitro defect of each cell type was restored by the respective expression of activated forms of these kinases. These findings reveal an unanticipated role for the 3BP2 adapter protein in osteoblast function and in coordinating bone homeostatic signals in both osteoclast and osteoblast lineages.

Introduction

3BP2 is an adapter protein that contains an N-terminal pleckstrin homology (PH) domain, a proline-rich stretch that binds to Src homology 3 (SH3) domain–containing proteins, and a C-terminal SH2 domain that binds to phosphotyrosine residues (1). 3BP2 was initially identified as a binding protein of the tyrosine kinase Abl (2). Work from our lab and others has identified the Src family kinases (SFKs), Syk, and the Vav family of Rho guanine nucleotide exchange factors (GEFs) as 3BP2-binding partners (1), all of which are known to play important roles in osteoclast function (3–5). Cherubism is a dominantly inherited syndrome characterized by excessive maxillary and mandibular bone resorption that is associated with activated osteoclasts and inflammatory cells creating interosseous cystic lesions (6). Single missense mutations in the gene encoding the adapter protein 3BP2 result in a gain-of-function alteration in the protein and is associated with the majority of cherubism patients (7). A mouse model that harbors 2 copies of a cherubism allele develops severe osteoporosis associated with highly activated osteoclasts (8).

In order to elucidate the role of the wild-type form of 3BP2 in bone homeostasis, we analyzed loss-of-function mutant mice. As distinct from the osteoporotic phenotype of mice expressing the cherubism gain-of-function form of 3BP2 associated with active osteoclasts, we uncovered a complex bone phenotype in mice lacking 3BP2 characterized by loss-of-function in both the osteoclast and osteoblast lineages resulting in net decreased bone mineral density and reduced mechanical bone strength. We show that in vivo osteoclast function is impaired in SH3-domain binding protein 2–knockout (*Sh3bp2*$^{-/-}$) mice. 3BP2-deficient osteoclasts spread poorly and are unable to effectively degrade dentine matrix in vitro. Src activation in response to integrin stimulation is defective in *Sh3bp2*$^{-/-}$ osteoclasts, and these osteoclasts poorly organize podosome belts.

In addition to defective osteoclastogenesis, we identified an unanticipated role for 3BP2 in osteoblast-dependent bone deposition. Bone formation rate (BFR) is greatly reduced in the 3BP2-deficient mice, and *Sh3bp2*$^{-/-}$ osteoblasts fail to form mineralized nodules in vitro. Because of the interdependent interactions between osteoblasts and osteoclasts, we have generated bone marrow chimeras, which demonstrate the autonomous defect within the osteoclast and osteoblast compartments in vivo.

Finally, we show that 3BP2 binds to the Abl tyrosine kinase SH3 domain and functions as an activating ligand for Abl, both in vitro and in vivo. We demonstrate that the osteoblast defect observed in the *Sh3bp2*$^{-/-}$ osteoblasts can be rescued by activating an ectopic form of Abl. These data demonstrate that 3BP2 is a unique regulator of osteoclast and osteoblast lineages, which are both necessary for normal bone homeostasis.

Results

Bone mass and bone strength are decreased in Sh3bp2$^{-/-}$ *mice.* To elucidate the role of 3BP2 in bone homeostasis, we analyzed the bone characteristics of 3BP2-deficient mice (9). Staining of tibia from 12-week-old *Sh3bp2*$^{-/-}$ mice with H&E revealed severe trabecular bone loss compared with wild-type mice (Figure 1A). Three-dimensional reconstruction of the femora using microcomputed tomography (μCT) showed a 47% loss of trabecular bone volume in the

Conflict of interest: The authors have declared that no conflict of interest exists.
Citation for this article: *J Clin Invest.* 2011;121(8):3244–3257. doi:10.1172/JCI45843.

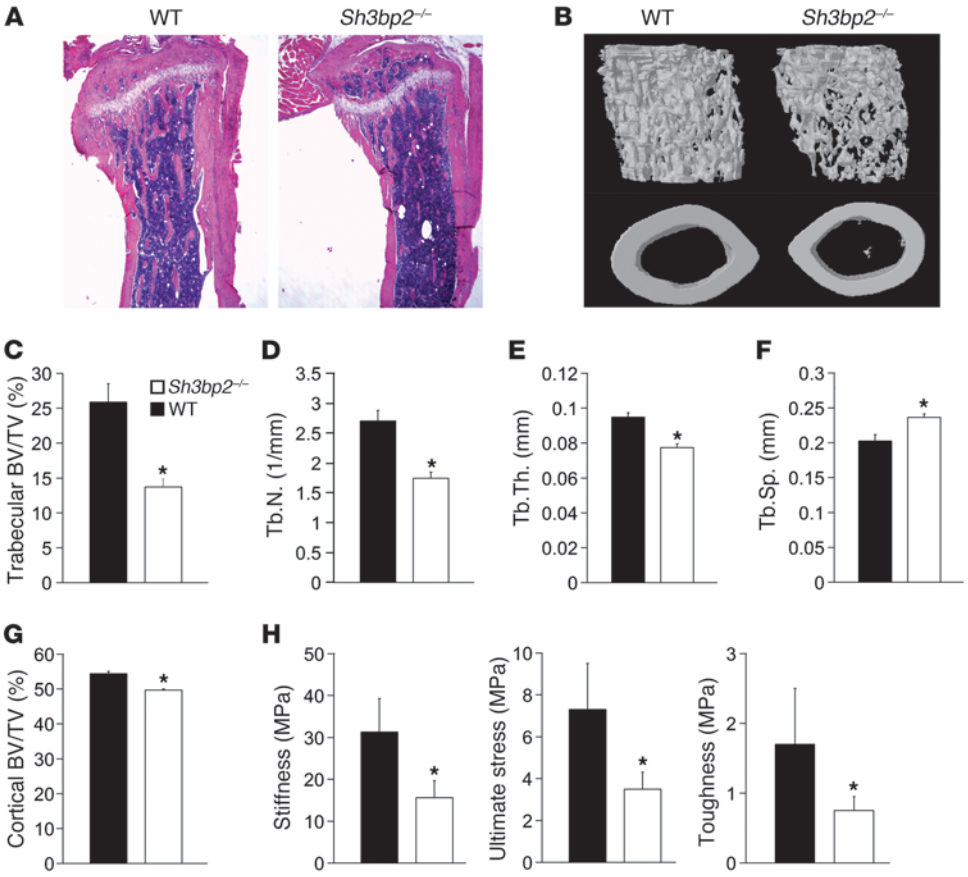

Figure 1
Decreased bone density and strength in 12-week-old *Sh3bp2*$^{-/-}$ mice. (**A**) H&E staining of tibia from 12-week-old *Sh3bp2*$^{-/-}$ and wild-type mice. (**B**) μCT reconstruction of the trabecular region below the distal femur growth plate (upper panel) and the cortical region of midshaft femurs (lower panel) of *Sh3bp2*$^{-/-}$ and wild-type mice. μCT-derived measurements of (**C**) BV/TV, (**D**) trabecular number (Tb.N), (**E**) trabecular thickness (Tb.Th), and (**F**) trabecular separation (Tb.Sp). $n = 9$; $^*P < 0.05$. (**G**) μCT-derived measurements of the cortical bone volume fraction (BV/TV). $n = 12$; $^*P < 0.05$. (**H**) Mechanical testing of vertebrae from wild-type and *Sh3bp2*$^{-/-}$ mice. $n = 5$; $^*P < 0.05$. Data are presented as mean ± SEM.

3BP2-deficient mice compared with sex- and age-matched controls as a consequence of decreased numbers of trabeculae and a reduction in trabecular thickness (Figure 1, B–E). Trabecular separation was increased in the *Sh3bp2*$^{-/-}$ mice compared with controls (Figure 1F). The loss in trabecular bone volume and architecture was not observed in younger mice at age 4 weeks, suggesting the phenotype is acquired during skeletal maturation (Supplemental Figure 1; supplemental material available online with this article; doi:10.1172/JCI45843DS1). Quantification of the cortical bone volume showed a small but significant decrease in 3BP2-deficient mice compared with wild-type littermates (Figure 1G).

To determine whether the loss of trabecular architecture observed in *Sh3bp2*$^{-/-}$ mice correlated with reduction in bone strength, we examined the mechanical properties of the bone from *Sh3bp2*$^{-/-}$ and wild-type mice. Uniaxial compression of vertebrae demonstrated that Young modulus, the ultimate stress-to-fracture, and the toughness of the bone were all reduced by approximately 50% in *Sh3bp2*$^{-/-}$ compared with their wild-type counterparts (Figure 1H).

Impaired bone resorption in Sh3bp2$^{-/-}$ *mice*. To elucidate the cause for bone loss in 3BP2-deficient mice, we first analyzed the osteoclast compartment in these mice. Histomorphometric analysis showed an increase in osteoclast surface relative to total bone surface (OcS/BS) and a trend for higher osteoclast number per bone surface (N.Oc/BS) in 3BP2-deficient mice (Figure 2, A and B). The ratio of trabecular bone volume to total volume (BV/TV) in femora bone sections was lower by 27% in the 3BP2-deficient mice compared with wild-type mice, consistent with the μCT analysis (Figure 2C). The elevated OcS/BS ratio observed in the knockout therefore may simply be a reflection of diminished BV/TV. The number of nuclei per osteoclast (N.Nuclei/Oc) in tartrate-resistant acid phosphatase–stained (TRAP-stained) sections was similar in wild-type and 3BP2-deficient mice (Figure 2D). *Tnfsf11* (RANKL) and its antagonist *Tnfsf11b* (osteoprotegerin) were expressed at similar levels in wild-type and *Sh3bp2*$^{-/-}$ bones, suggesting that the trend of increased osteoclast numbers was not a result of altered RANKL or osteoprotegerin expression (Figure 2, E and F). However, serum CTX-I levels, a measure of in vivo osteoclast function, were reduced in *Sh3bp2*$^{-/-}$ mice compared with wild-type mice (Figure 2G). We imaged osteoclasts in situ using transmission electron microscopy (TEM) to quantify cells with mature ruffled borders (Figure 2H). We observed that fewer 3BP2-deficient osteoclasts formed mature ruffled borders compared with wild-type osteoclasts (57% of *Sh3bp2*$^{-/-}$ osteoclasts versus 85% of wild-type osteoclasts) (Figure 2I). The 33% reduction in the frequency of ruffled borders observed in 3BP2-deficient osteoclasts together with the reduction in CTX-I serum levels suggest that, as distinct from osteoclasts derived from cherubism mice, 3BP2-deficient osteoclasts have reduced activity in vivo. In addition, we observed that *Sh3bp2*$^{-/-}$ mice manifested a modest reduction in body length at 5 months of age compared with wild-type mice, consistent with the short stature often observed in some mice models with an osteoclast defect (refs. 10, 11, and Figure 2J).

Finally, in order to examine the intrinsic influence of 3BP2-deficient osteoclasts on bone mass, we transplanted wild-type or *Sh3bp2*$^{-/-}$ bone marrow into sublethally irradiated wild-type recipient mice. Reconstitution of wild-type recipient mice with wild-

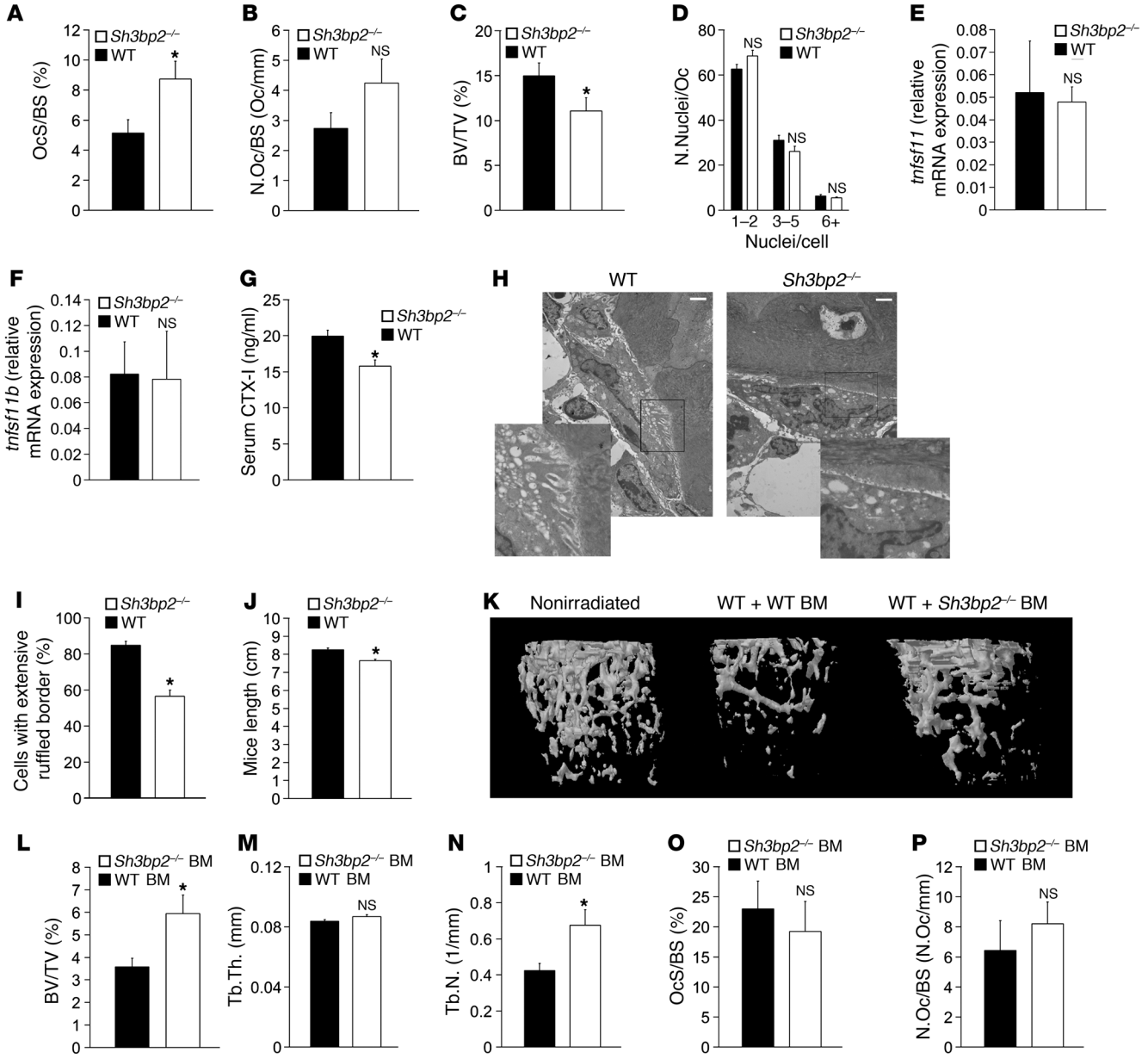

Figure 2

Impaired bone resorption by *Sh3bp2*$^{-/-}$ osteoclasts. Histomorphometric analysis of (**A**) OcS/BS, (**B**) N.Oc/BS, and (**C**) BV/TV in 12-week-old mice. $n = 6$; $^*P < 0.05$. (**D**) Analysis of N.Nuclei/Oc in tibias of 12-week-old mice. Osteoclasts were sorted into groups with 1–2, 3–5, and 6+ N.Nuclei/Oc. $n = 6$. Quantitative PCR analysis of *tnfsf11* (**E**) and *tnfsf11b* (**F**) transcript levels in the bones of 12-week-old wild-type and *Sh3bp2*$^{-/-}$ mice. $n = 5$. (**G**) ELISA measurement of basal serum CTX-I levels in 12-week-old wild-type and *Sh3bp2*$^{-/-}$ mice. $n = 5$; $^*P < 0.01$. (**H**) TEM of vertebral sections from 4-week-old wild-type and *Sh3bp2*$^{-/-}$ mice showing representative osteoclasts exhibiting mature and attenuated ruffled borders from wild-type or *Sh3bp2*$^{-/-}$ mice, respectively. Scale bars: 2 μm. (**I**) Quantification of osteoclasts with mature ruffled borders. $n = 50$ osteoclasts from 3 wild-type and 3 *Sh3bp2*$^{-/-}$ mice (approximately 15 osteoclasts/mouse); $P < 0.01$. (**J**) Length measurements of 5-month-old wild-type or *Sh3bp2*$^{-/-}$ mice. The distance between the snout and anus is shown. $n = 15$ wild-type and 13 *Sh3bp2*$^{-/-}$ mice; $P < 0.01$. (**K**) μCT reconstruction of the femora of 16-week-old wild-type recipient mice, 8 weeks following the transfer of wild-type or *Sh3bp2*$^{-/-}$ bone marrow. Nonirradiated control is shown on the left. (**L**–**N**) μCT-derived measurements of (**L**) BV/TV, (**M**) Tb.Th, and (**N**) Tb.N. $n = 8$; $^*P < 0.05$. (**O** and **P**) Histomorphometric analysis of (**O**) OcS/BS and (**P**) N.Oc/BS in the tibias of 16-week-old wild-type recipient mice, 8 weeks following the transfer of wild-type or *Sh3bp2*$^{-/-}$ bone marrow is shown. $n = 4$; $^*P < 0.05$. Data are presented as mean ± SEM.

type bone marrow resulted in a 40% reduction in the trabecular bone volume relative to nonirradiated control mice, demonstrating the negative impact radiation has on bone homeostasis (12). When 3BP2-deficient bone marrow from 8-week-old male mice was transferred into 8-week-old male wild-type recipient mice, we observed a 40% higher trabecular bone mass relative to mice injected with wild-type bone marrow 8 weeks after transplantation (Figure 2, K and L). Although trabecular thickness showed

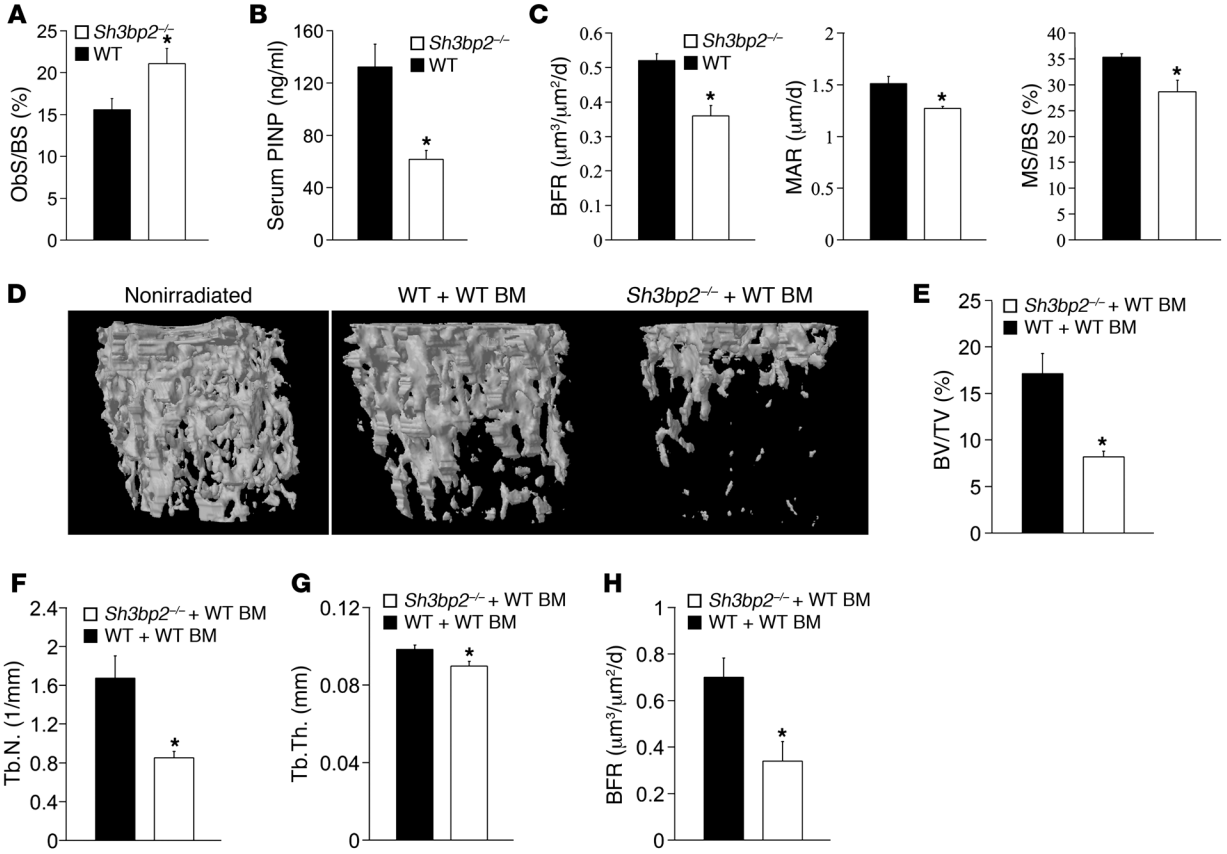

Figure 3

Impaired bone deposition in *Sh3bp2*$^{-/-}$ mice. (**A**) Histomorphometric analysis of osteoblast surface to bone surface (ObS/BS). $n = 6$; $^*P < 0.05$. (**B**) Serum PINP levels in wild-type and *Sh3bp2*$^{-/-}$ 12-week-old mice as measured by ELISA. $n = 9$; $^*P < 0.01$. (**C**) Dynamic histomorphometric analysis of bones from 12-week-old wild-type and *Sh3bp2*$^{-/-}$ mice. Measurement of BFR, MAR, and MS/BS is shown. $n = 5$; $^*P < 0.01$. (**D**) μCT reconstruction of the femurs of 16-week-old wild-type or *Sh3bp2*$^{-/-}$ mice, 8 weeks following the transfer of wild-type bone marrow. Nonirradiated control is shown on the left. μCT-derived measurements of (**E**) BV/TV, (**F**) Tb.N, and (**G**) Tb.Th. $n = 8$ mice; $^*P < 0.05$. (**H**) Dynamic histomorphometric analysis of tibias from 16-week-old wild-type or *Sh3bp2*$^{-/-}$ mice, 8 weeks following the transfer of wild-type bone marrow. Measurement of BFR is shown. $n = 3$, $^*P < 0.05$. Data are presented as mean ± SEM.

no difference between the 2 recipient groups (Figure 2M), there was a 38% increase in trabeculae numbers (Figure 2N). Histomorphometric analysis showed no statistical difference in the ratio of osteoclast surface to total bone surface or osteoclast number per bone surface in the recipient mice, which received 3BP2-deficient or wild-type donor bone marrow cells, suggesting that the increase in bone volume was a result of osteoclast dysfunction rather than a decrease in osteoclast numbers (Figure 2, O and P). Taken together, these results confirm an intrinsic bone-resorbing defect of 3BP2-deficient osteoclasts in vivo.

Impaired bone formation in 3BP2-deficient mice. Our data demonstrate that the osteoporotic phenotype observed in *Sh3bp2*$^{-/-}$ mice cannot be attributed to enhanced osteoclast activity and raises the possibility that osteoblast function may be impaired in the mutant mice. We next compared the osteoblast compartment in wild-type and *Sh3bp2*$^{-/-}$ mice. Histomorphometric analysis showed a higher osteoblast surface to total bone surface in *Sh3bp2*$^{-/-}$ mice compared with littermate controls (Figure 3A). Serum levels of type I collagen aminoterminal propeptide of type I procollagen (PINP), a sensitive and specific marker of bone formation. were lower by 54% in *Sh3bp2*$^{-/-}$ mice compared with their wild-type counterparts, indicating a profound decrease in bone formation (Figure 3B). Moreover, dynamic bone histomorphometric analysis after calcein-green xylenol-orange double labeling confirmed a substantial decrease in the BFR (30%), mineral apposition rate (MAR) (16%), and mineralizing surface to bone surface (MS/BS) (19%) in the mutant mice compared with wild-type controls (Figure 3C).

Since osteoclast and osteoblast development and activity are coupled through reciprocal paracrine interactions in vivo, we wanted to isolate the intrinsic defect in the osteoblast compartment. For this purpose, we generated bone marrow chimeras to determine the activity of the osteoblast compartment in *Sh3bp2*$^{-/-}$ mice in vivo. Wild-type bone marrow was transferred into either wild-type or 3BP2-deficient irradiated recipient mice and trabecular bone volume measured by μCT 8 weeks after transfer. We again observed reduction in the trabecular bone volume relative to nonirradiated control mice due to the effect of radiation on bone density. The transfer of wild-type bone marrow into 3BP2-deficient mice, however, resulted in a further loss of 53% in trabecular volume compared with wild-type recipient mice (Figure 3, D and E) accompanied by a 50% reduction in trabeculae numbers (Figure 3F) and 10% reduction in trabeculae thickness in *Sh3bp2*$^{-/-}$ mice

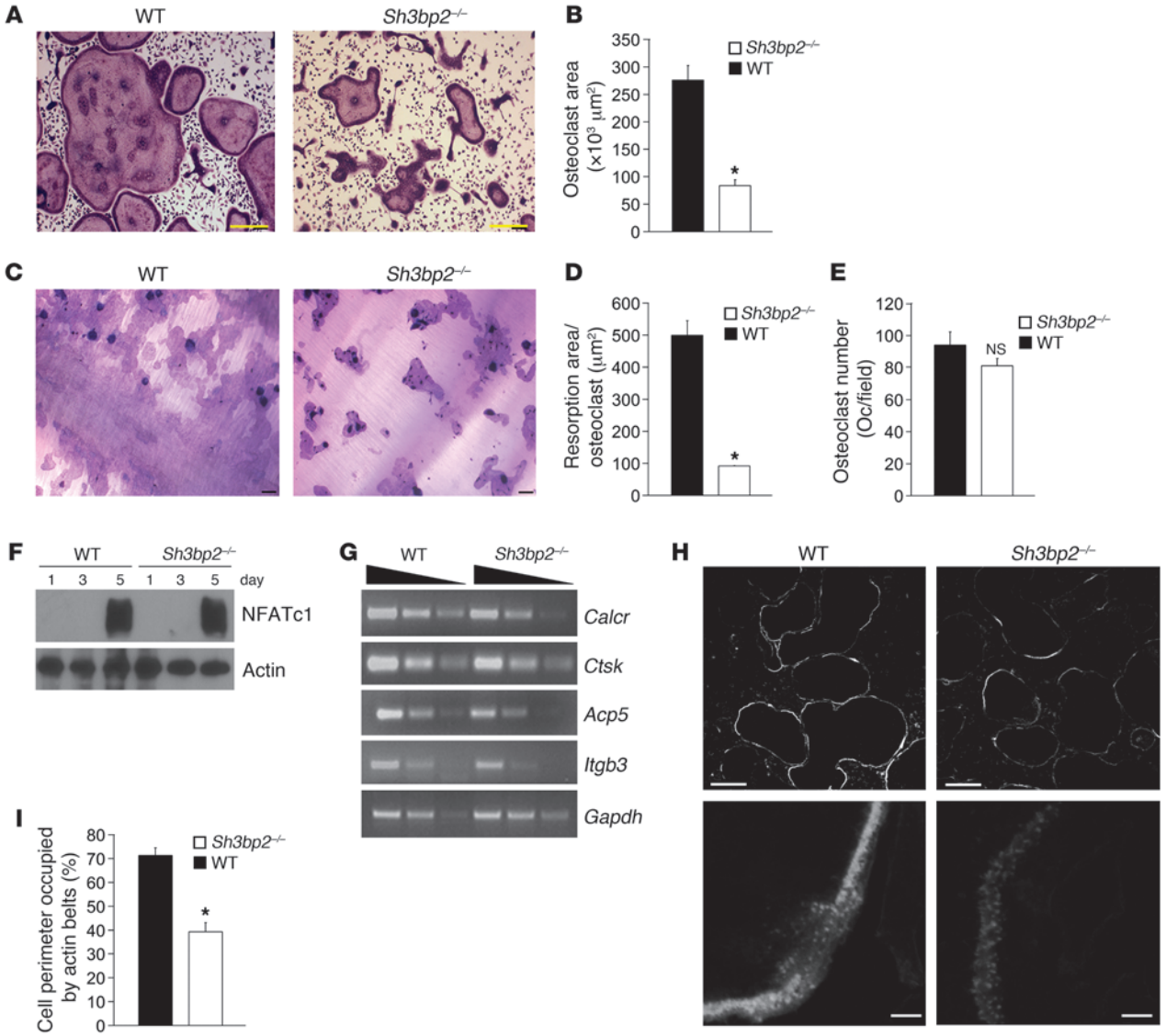

Figure 4

3BP2 is required for osteoclast function but not differentiation. (**A**) TRAP staining of osteoclasts derived from wild-type and *Sh3bp2*$^{-/-}$ BMMs cultured for 5 days. Scale bars: 100 μm. (**B**) Quantification of osteoclast area. $n = 4$; $^*P < 0.01$. (**C**) Resorptive pits formation assay on dentin discs of wild-type or *Sh3bp2*$^{-/-}$ BMMs cultured for 7 days. (**D**) Comparison of wild-type and *Sh3bp2*$^{-/-}$ osteoclast resorption pit area. $n = 3$; $^*P < 0.01$. (**E**) Quantification of TRAP-positive and multinucleated (>3 nuclei/cell) osteoclasts derived from wild-type and *Sh3bp2*$^{-/-}$ BMMs cultured for 3 days. (**F**) Western blot analysis of NFATc1 protein levels in wild-type and *Sh3bp2*$^{-/-}$ BMMs grown at different time intervals. (**G**) Semiquantitative PCR analysis of *Calcr*, *Ctsk*, *Acp5*, and *Itgb3* expression in wild-type and *Sh3bp2*$^{-/-}$ osteoclasts grown for 5 days. *Gapdh* mRNA levels served as the normalization reference. (**H**) Phalloidin staining of wild-type and 3BP2-deficient osteoclasts cultured for 5 days. Scale bars: 100 μm (upper panels); 5 μm (lower panels). (**I**) The percentage of cell perimeter occupied by high-density podosome belts in **H** was quantified. $^*P < 0.01$. Data are presented as mean ± SEM.

(Figure 3G). In keeping with the bone loss phenotype observed above, we measured a 30% reduction in the BFR in chimeric 3BP2-deficient mice reconstituted with normal bone marrow compared with the wild-type chimeric control mice (Figure 3H). These results demonstrate that an intrinsic defect in bone formation within the osteoblast compartment is the cause for the osteoporotic phenotype observed in the 3BP2-deficient mice.

3BP2 is required for osteoclast function but not differentiation. We next examined the capacity of bone marrow–derived monocytes (BMMs) from wild-type or *Sh3bp2*$^{-/-}$ mice to undergo osteoclastogenesis in vitro. TRAP-positive osteoclasts from *Sh3bp2*$^{-/-}$ mice were small and irregularly shaped (Figure 4A), with 3-fold reduced surface area (Figure 4B), suggesting a cytoskeletal defect.

We tested the capacity of *Sh3bp2*$^{-/-}$ osteoclasts to degrade dentine matrix and observed that these osteoclasts failed to spread on the dentine surface with impaired resorptive activity (Figure 4C). The resorption pit area per cell of the *Sh3bp2*$^{-/-}$ osteoclasts was reduced by 80% compared with wild-type controls (Figure 4D).

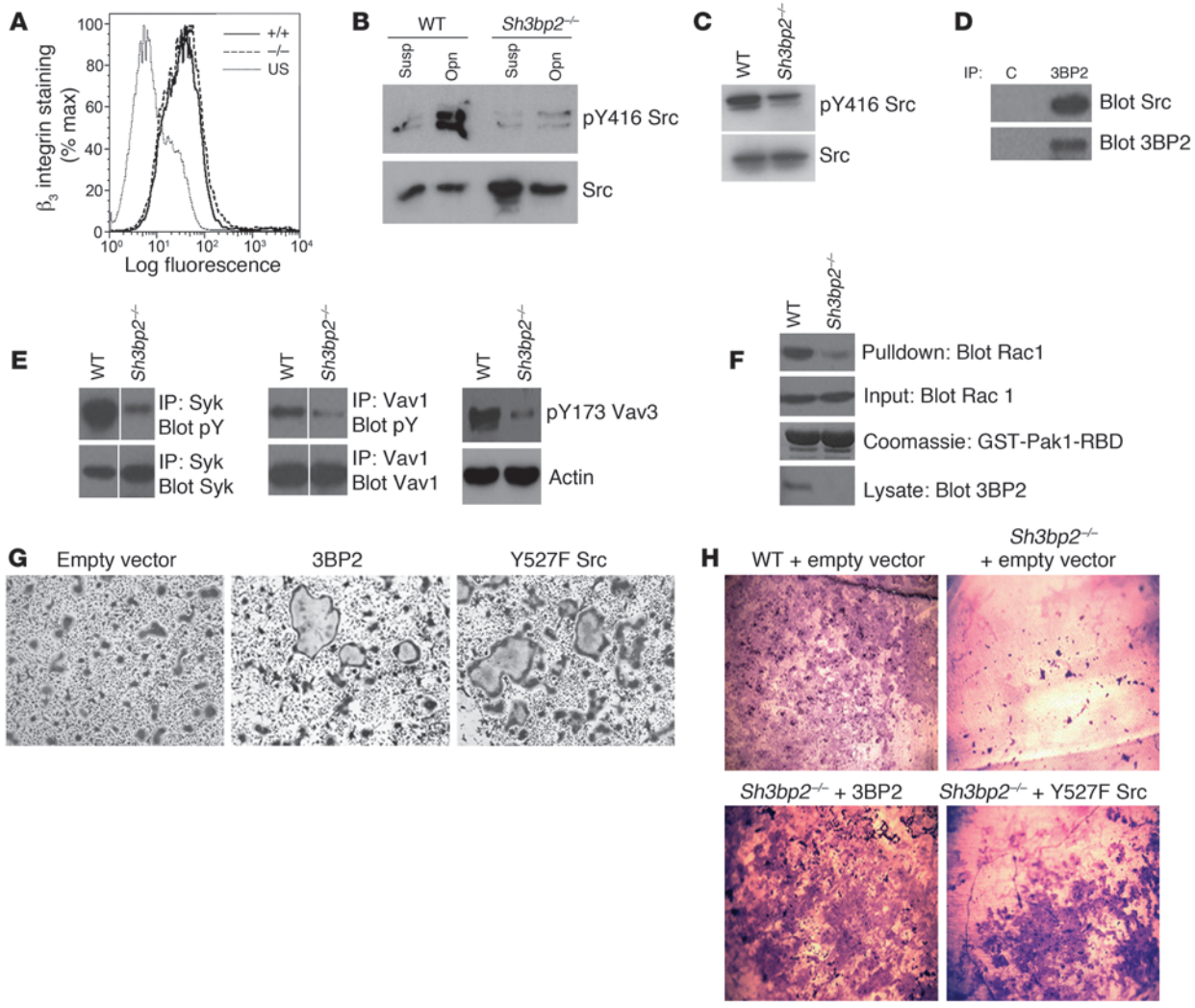

Figure 5

Integrin-mediated activation of Src is defective in *Sh3bp2*$^{-/-}$ osteoclasts. (**A**) FACS analysis of β_3 integrin expression on the surface of wild-type or *Sh3bp2*$^{-/-}$ osteoclasts cultured for 3 days. *Sh3bp2*$^{-/-}$ (–/–), wild-type (+/+), and unstained (US). (**B**) Western blot analysis of active Src levels in wild-type or 3BP2-deficient preosteoclasts cultured for 3 days, lysed in suspension, or 1 hour after plating on osteopontin (Opn). Lysates were probed with anti-Src or anti–Src pY^{416} antibodies. (**C**) Western blot analysis of active Src levels in wild-type and *Sh3bp2*$^{-/-}$ osteoclasts cultured for 5 days. Lysates were probed with anti-Src and anti–Src pY^{416} antibodies. (**D**) Coimmunoprecipitation of endogenous complexes of 3BP2 with Src in Raw264.7 cells cultured for 5 days. C, IgG control. (**E**) Western blot analysis of activated Syk, Vav1, and Vav3 in wild-type and *Sh3bp2*$^{-/-}$ BMMs cultured for 5 days. Syk, Vav1, and Vav3 proteins were immunoprecipitated and probed for phosphotyrosine or with an anti–Vav3 pY^{173} antibody. (**F**) Rac1GTP was coprecipitated from lysates derived from wild-type or *Sh3bp2*$^{-/-}$ osteoclasts using immobilized recombinant Pak1-RBD protein and probed with an anti-Rac1 monoclonal antibody. (**G**) *Sh3bp2*$^{-/-}$ osteoclasts were infected by a retrovirus expressing either 3BP2 or Src Y527F. Empty vector was used as a control. Following infection, cells were cultured for 5 days and then stained for TRAP. (**H**) As in **G**, infected cells were plated on dentin and cultured for 10 days. Dentin chips were stained with Toluidine to reveal resorption pits. Original magnification, ×10 (**G**); ×5 (**H**). Data are presented as mean ± SEM.

These findings confirm an autonomous defect in 3BP2-deficient osteoclasts cultured in vitro.

In order to determine whether 3BP2 deficiency was associated with a failure of osteoclast lineage commitment, we showed that there was no difference in the numbers of TRAP-positive multinucleated cells in wild-type and *Sh3bp2*$^{-/-}$ after 3 days of culture (Figure 4E) nor evidence of accelerated apoptosis as measured by caspase-3 cleavage products (Supplemental Figure 2A). We next examined the induction of NFATc1 and NFATc1-regulated genes known to drive the osteoclastogenic program. We observed that NFATc1 protein and mRNA levels were similar in wild-type and 3BP2-deficient osteoclast cultures (Figure 4F and Supplemental Figure 2B). The NFATc1-induced genes *Calcr*, *Ctsk*, *Acp5*, and *Itgb3* were expressed at similar levels in wild-type and 3BP2-deficient osteoclasts (Figure 4G). NFATc1 is regulated by the activation of PLCγ2 in osteoclasts (13). Moreover, PLCγ2 phosphorylation is increased following 3BP2 overexpression (14). We examined the phosphorylation status of PLCγ2 in osteoclasts and showed that the levels of phospho-PLCγ2 were similar in wild-type and *Sh3bp2*$^{-/-}$ mice during in vitro osteoclastogenesis (Supplemental

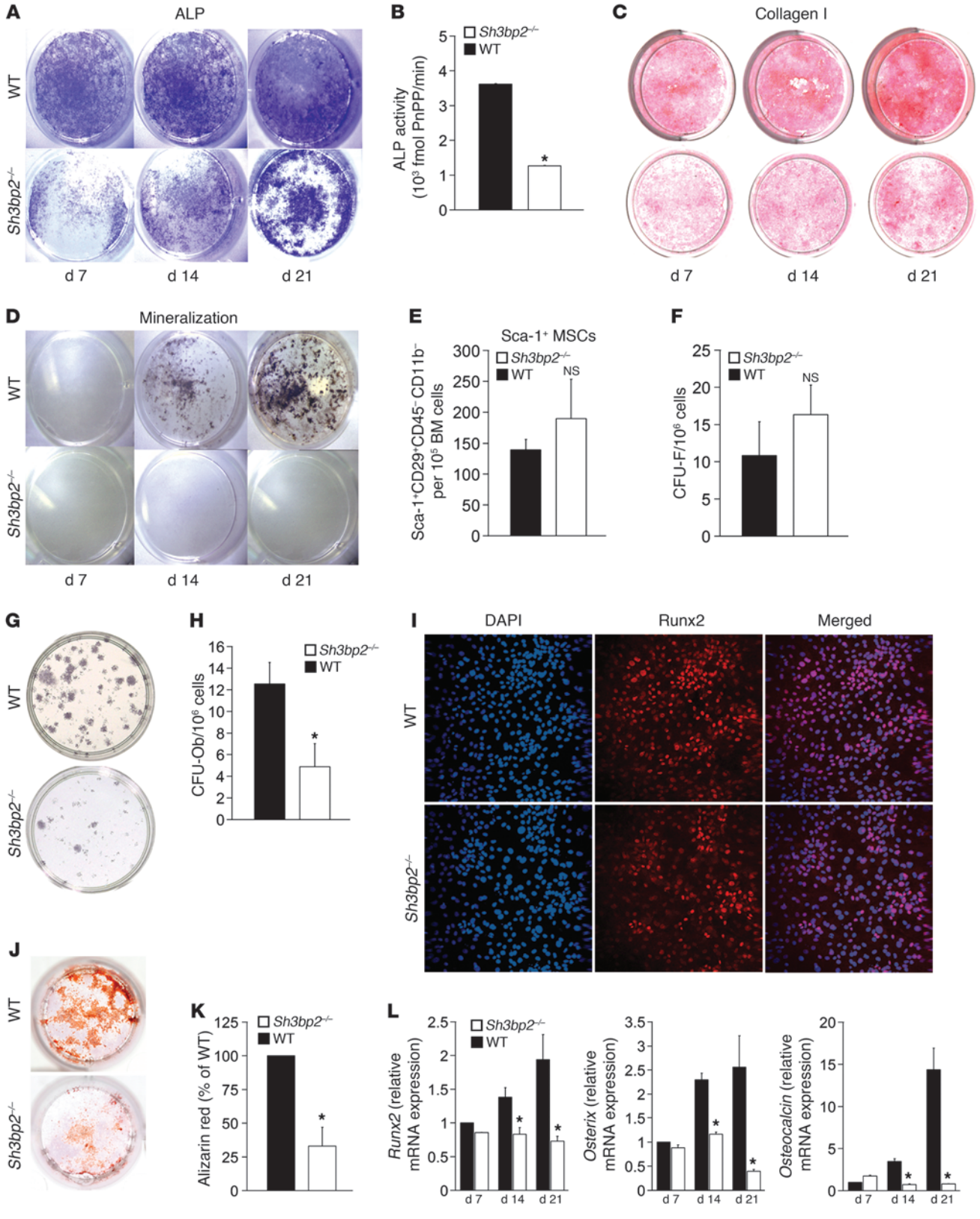
A
ALP
WT
Sh3bp2-/-
d 7
d 14
d 21
B
Sh3bp2-/-
WT
ALP activity
(10³ fmol PnPP/min)
C
Collagen I
d 7
d 14
d 21
D
Mineralization
WT
Sh3bp2-/-
d 7
d 14
d 21
E
Sca-1+ MSCs
Sh3bp2-/-
WT
NS
Sca-1+CD29+CD45-CD11b-
per 10⁵ BM cells
F
Sh3bp2-/-
WT
NS
CFU-F/10⁶ cells
G
WT
Sh3bp2-/-
H
Sh3bp2-/-
WT
CFU-Ob/10⁶ cells
I
DAPI
Runx2
Merged
WT
Sh3bp2-/-
J
WT
Sh3bp2-/-
K
Sh3bp2-/-
WT
Alizarin red (% of WT)
L
Sh3bp2-/-
WT
Runx2 (relative mRNA expression)
Osterix (relative mRNA expression)
Osteocalcin (relative mRNA expression)
d 7
d 14
d 21

Figure 6
Impaired osteoblast maturation in *Sh3bp2*$^{-/-}$ mice. (**A**) In vitro osteoblast maturation assay. Bone marrow–derived stromal cells were cultured for 21 days and stained for ALP after 7, 14, or 21 days of culture. (**B**) Quantification of ALP activity after 14 days of culture. $n = 9$; $^*P < 0.05$. (**C**) Collagen I deposition as determined by picric acid staining after 7, 14, and 21 days of culture. (**D**) Mineralized nodule formation as determined by von Kossa staining after 7, 14, and 21 days of culture. (**E**) FACS analysis of Sca-1$^+$CD29$^+$CD45$^-$CD11b$^-$ skeletal stem cells from 12- to 13-week-old wild-type or *Sh3bp2*$^{-/-}$ mice. $n = 7$. (**F**) Quantification of CFU-F from wild-type and *Sh3bp2*$^{-/-}$ bone marrow–derived adherent cells cultured for 2 weeks. $n = 12$. (**G**) ALP staining of CFU-F cultured for 28 days. (**H**) Quantification of CFU-Ob from **G**. $n = 6$; $^*P < 0.05$. (**I**) Immunofluorescence staining for Runx2 (red) or nuclei (DAPI). Original magnification, ×10. (**J**) Decreased mineralized nodules of *Sh3bp2*$^{-/-}$ calvarial-derived osteoblasts cultured for 21 days and stained with Alizarin red (**K**). Quantification of calvarial osteoblast mineralized nodules in **I**. $n = 6$; $^*P < 0.01$. (**L**) Quantitative PCR of *runx2*, *osterix*, and *osteocalcin* transcript levels in calvarial osteoblasts cultured for 21 days. $n = 3$; $^*P < 0.05$. Data are presented as mean ± SEM.

Figure 2C). Finally, the nuclear localization of the osteoclastogenic transcription factors NFATc1, NF-κB, and c-Fos in 3BP2-deficient osteoclasts was comparable to that of wild-type osteoclasts (Supplemental Figure 2D). These data suggest that the osteoclastogenic program proceeds normally in the absence of 3BP2.

Bone marrow monocytes undergo fusion to form multinucleated osteoclasts through a receptor-mediated process via DC-STAMP (15) and Atp6v0d2 (16, 17). We showed that 3BP2-deficient osteoclasts express both DC-STAMP and Atp6v0d2 at normal levels (Supplemental Figure 2E). Together with the similar N.Nuclei/Oc observed in the wild-type and 3BP2-deficient osteoclasts in vivo (Figure 2D), these results suggest that 3BP2 is not required for normal fusion of osteoclast precursors.

Staining of the actin cytoskeleton with Texas red–conjugated phalloidin showed well-developed podosome belts in a continuous ring around the cell periphery in wild-type osteoclasts, whereas actin staining of podosome structures was diffuse in *Sh3bp2*$^{-/-}$ osteoclasts with a 50% reduction in the cell perimeter occupied by high-density podosome belts (Figure 4, H and I). These data demonstrate that 3BP2 is required for actin cytoskeletal organization and normal osteoclast function both in vitro and in vivo and that the osteoporotic phenotype observed in *Sh3bp2*$^{-/-}$ mice cannot be attributed to defects within the osteoclast compartment.

Integrin-mediated activation of Src is defective in Sh3bp2$^{-/-}$ *osteoclasts*. Integrin-mediated adhesion to bone matrix is required for osteoclast differentiation, actin reorganization, and cellular polarization. $\alpha_v\beta_3$ integrin is specifically required for osteoclast function (18–22). We analyzed the level of β_3 cell surface expression in wild-type and *Sh3bp2*$^{-/-}$ osteoclasts by flow cytometry and determined that β_3 integrin levels were unaffected in the knockout osteoclasts (Figure 5A).

Integrin engagement by matrix elements within bone results in activation of Src tyrosine kinase, which is required for normal osteoclast function (3, 23, 24). Src can bind directly to the carboxy-terminal region of the β_3 tail and can be activated by integrin clustering (25). We assessed Src activation by Western blotting using phospho-Y416 antibodies, which recognize the activation loop tyrosine, as a surrogate measure of Src activity following replating of wild-type or *Sh3bp2*$^{-/-}$ osteoclasts on osteopontin, an $\alpha_v\beta_3$ ligand, and observed that Src was poorly activated in *Sh3bp2*$^{-/-}$ osteoclasts (Figure 5B). We also noted that *Sh3bp2*$^{-/-}$ osteoclasts grown continuously in RANKL and CSF-1 failed to fully activate Src compared with wild-type cells (Figure 5C). 3BP2 binds to the Src family kinase members Fyn and Lyn in immune cell overexpression systems (26, 27). We wanted to determine whether Src and 3BP2 form a physical complex in developing osteoclasts. Western blot analysis of 3BP2 immune complexes derived from cultured Raw264.7 osteoclasts demonstrated that 3BP2 and Src form an endogenous protein complex (Figure 5D). These data show that 3BP2 and Src form a signaling module required for optimal Src activation in response to $\alpha_v\beta_3$ integrin activation in osteoclasts.

$\alpha_v\beta_3$ engagement in osteoclasts leads to the activation of the Syk tyrosine kinase (28), the Vav3 GEF, and RacGTPase (5), all of which are required for actin organization and osteoclast function. Importantly, both Syk (29) and Vav3 (30) are established 3BP2-binding partners (1). We tested to determine whether Syk, Vav1, Vav3, and Rac1 are normally activated in the absence of 3BP2. We observed that cultured *Sh3bp2*$^{-/-}$ osteoclasts failed to induce maximal Syk or Vav1/3 tyrosine phosphorylation compared with wild-type osteoclasts (Figure 5E). Since Vav3 is critical for Rac activation in osteoclasts, we assessed the activation of Rac1 using an RBD pull-down assay and observed that Rac1GTP was greatly reduced in *Sh3bp2*$^{-/-}$ osteoclasts compared with wild-type cells (Figure 5F). The similarity in the in vitro osteoclast defect observed in $\alpha_v\beta_3$, Src, Syk, Vav3, and 3BP2-knockout mice suggests that 3BP2 may be part of a common signaling pathway with these proteins. Since Src is considered to be a proximal component of this pathway (4), we next wanted to determine whether an activated form of Src was sufficient to restore the function of 3BP2-null osteoclasts. *Sh3bp2*$^{-/-}$ BMMs were infected with a retrovirus expressing Src-Y527F and cultured for 5 days or for 10 days on dentin discs. *Sh3bp2*$^{-/-}$ BMMs infected with the Src-Y527F retrovirus but not mock controls regained the capacity to form large multinucleated osteoclasts and to efficiently resorb dentin as compared with wild-type mock-infected cells (Figure 5, G and H). These data identify 3BP2 as an unrecognized component of integrin-based signaling required for optimal Src activation in osteoclasts.

Impaired osteoblast maturation in 3BP2-deficient mice. Osteoblast differentiation and maturation is an ordered process marked by the sequential expression of alkaline phosphatase (ALP), subsequent collagen secretion, and mineral deposition. To determine whether 3BP2-deficient osteoblasts have a cell-autonomous defect in vitro, stromal cells from the bone marrow of wild-type and *Sh3bp2*$^{-/-}$ mice were isolated, cultured in osteogenic medium for 21 days, and stained for ALP, collagen, and mineralized nodule formation. We observed diminished ALP staining and a reduction of 68% in ALP activity in the 3BP2 mutant cultured osteoblasts compared with wild-type controls (Figure 6, A and B). Collagen deposition (Figure 6C) and mineralized nodules (Figure 6D) were also severely impaired in the *Sh3bp2*$^{-/-}$ osteoblasts. These data indicate that 3BP2 is required for normal bone synthesis in vivo and for the development of functionally normal osteoblasts in vitro.

The diminished ALP activity and impaired matrix and mineralized nodule formation observed in the *Sh3bp2*$^{-/-}$ osteoblasts may be a reflection of fewer bone marrow–derived mesenchymal progenitors in the knockout mice. We measured the frequency of a TGF-β1–sensitive skeletal stem cell population defined by the cell surface markers Sca-1$^+$CD29$^+$CD45$^-$CD11b$^-$ (31) in *Sh3bp2*$^{-/-}$ mice. The frequency of Sca-1$^+$CD29$^+$CD45$^-$CD11b$^-$ cells in the bone marrow of *Sh3bp2*$^{-/-}$ mice was not statistically different from

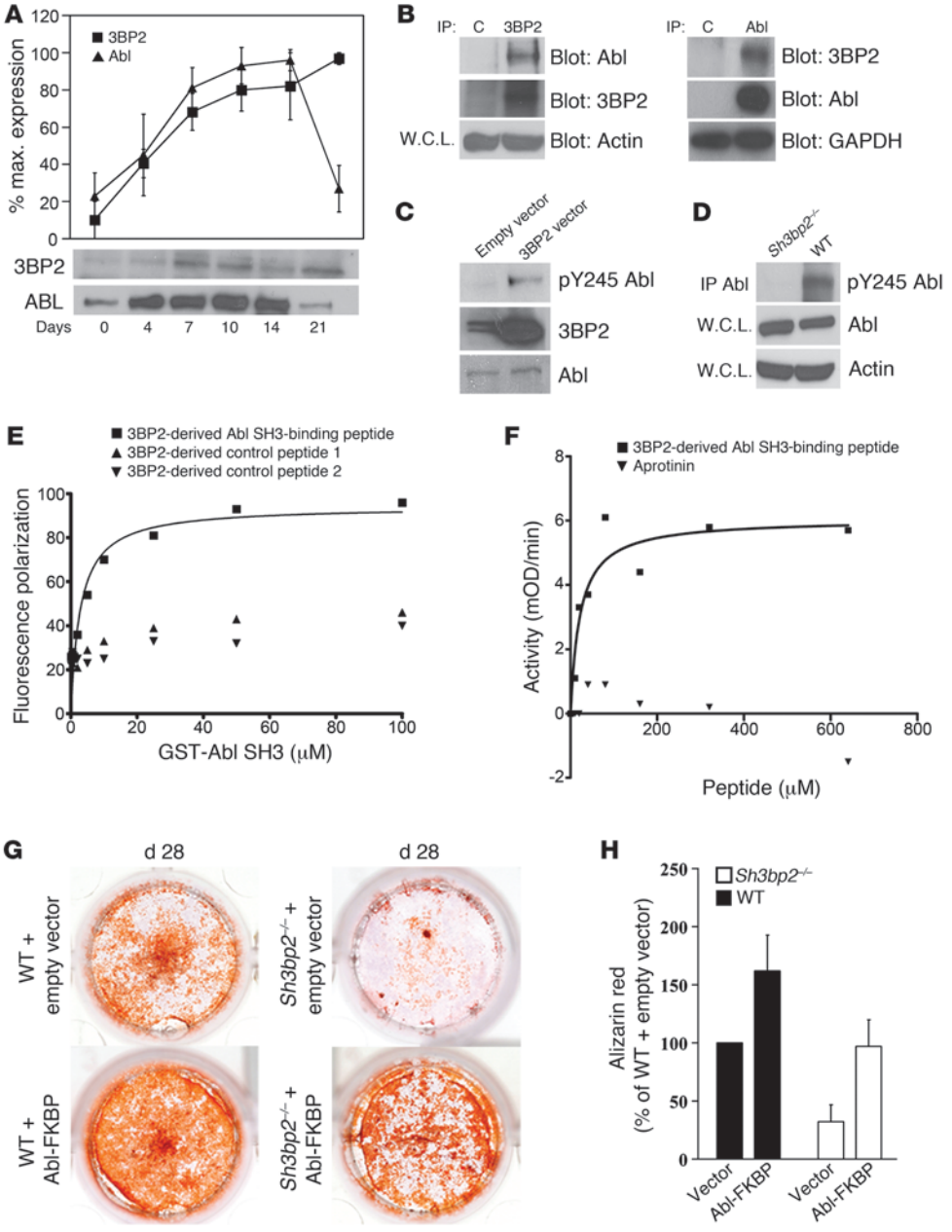

Figure 7

3BP2 is required for Abl activation in osteoblasts. (**A**) Abl and 3BP2 were immunoprecipitated and Western blotted, respectively, at various time points during differentiation of MC3T3 cells (n = 4). The blots were quantified by densitometry and relative values plotted. (**B**) Abl and 3BP2 were reciprocally coimmunoprecipitated from MC3T3 cells cultured for 14 days. Beads with nonrelevant polyclonal antibodies or isotype-matched monoclonal antibodies were used as controls. W.C.L., whole cell lysates; C, IgG control. (**C**) Lysates from MC3T3 infected with a 3BP2-expressing retroviral vector or an empty vector control were probed with an anti–Abl pY^{245} specific antibody. (**D**) Abl protein was immunoprecipitated from mineralizing wild-type or *Sh3bp2*$^{-/-}$ calvarial osteoblasts and probed with anti–Abl pY^{245} specific antibody. (**E**) Binding curve of the Abl SH3 domain to the FITC-conjugated 3BP2 diproline peptide, as measured by fluorescence polarization. 2 irrelevant 3BP2-derived peptides were used as negative controls. (**F**) The activity of recombinant SH3SH2 kinase Abl protein was measured in a continuous kinase assay in the presence of increasing concentrations of the 3BP2 diproline peptide or the Aprotinin-negative control peptide. The data in **E** and **F** are representative of 3 and 4 independent experiments, respectively. (**G**) Wild-type and *Sh3bp2*$^{-/-}$ calvarial-derived osteoblast progenitors were infected with the Abl-FKBP–expressing retroviral vector or an empty vector control and grown under osteogenic conditions in the presence of AP20187 for 28 days. Cells were then stained with alizarin red and quantified following elution (**H**), n = 18. Data are presented as mean ± SEM.

that of wild-type littermates (Figure 6E). We next measured the frequency of CFU fibroblasts (CFU-Fs) in the bone marrow of 12-week-old *Sh3bp2*$^{-/-}$ or wild-type mice and observed no significant differences in CFU-F numbers between the 2 strains (Figure 6F). To determine the ability of bone marrow stromal cells (BMSCs) to differentiate into ALP-positive osteogenic CFUs (CFU-Ob), we cultured CFU-F colonies in osteogenic medium for 28 days and observed 60% fewer mineralized nodules in *Sh3bp2*$^{-/-}$ BMSC cultures compared with wild-type controls (Figure 6, G and H). These data suggest that while 3BP2 is not required for determining the size of the mesenchymal progenitor pool in long bones, it is required for osteoblast lineage specification.

We next asked whether 3BP2 is also required for the maturation of calvarial-derived osteoblast progenitors, which are of paraxial mesoderm and neural crest origin (32). Calvarial osteoblast progenitors from wild-type or *Sh3bp2*$^{-/-}$ mice expressed similar levels of *Runx2*, a marker of early osteogenic progenitors (33), as measured by immunofluorescence staining or quantitative PCR (Figures 6I and Supplemental Figure 3), suggesting that calvarial-derived progenitor cell numbers were similar between the 2 strains. In order to determine whether neural crest–derived osteoblast progenitors can undergo normal maturation in the absence of 3BP2, we cultured calvarial cells for 21 days under osteogenic conditions. We observed that 3BP2-deficient osteoblast progenitors demonstrated a 65% reduction in mineralized nodule formation compared with wild-type controls (Figure 6, J and K). Moreover, the capacity of *Sh3bp2*$^{-/-}$ osteoblast progenitors to execute an osteogenic differentiation program during the maturation process, as measured by the induction of *Runx2*, *Osterix*, and *Osteocalcin* mRNA, was significantly reduced (Figure 6L). These data demon-

strate that 3BP2 regulates osteoblast maturation in both BMSCs and neural crest–derived progenitors.

3BP2 regulates Abl activation in osteoblasts. We hypothesized that the defect in osteoblastogenesis observed in the *Sh3bp2*$^{-/-}$ mice may be due to a defect in the regulation of the 3BP2-binding partner Abl (34), known to be required for normal osteoblast maturation (35). We analyzed the expression of 3BP2 and Abl proteins during in vitro osteoblast differentiation of the osteoblast cell line MC3T3-E1 (36). Abl protein levels increased significantly during the first fourteen days of differentiation and then declined toward basal levels as has previously been described (ref. 35 and Figure 7A). 3BP2 protein expression showed a similar pattern of induction, reaching the highest level after 14 days and maintaining expression thereafter (Figure 7A). In order to determine whether Abl and 3BP2 form a complex in differentiating osteoblasts, we probed MC3T3-E1 cells on day 14 of culture when mineralized nodule formation had commenced. We showed by reciprocal coimmunoprecipitation that endogenous 3BP2 and Abl form a stable protein complex in cells undergoing osteoblast maturation (Figure 7B). Abl exists in an inactive autoinhibited state in which the SH3 and SH2 domains bind through intramolecular interactions to the kinase domain and function as a "clamp" to maintain a conformer of low catalytic activity (37). Release of the SH3-SH2 domain from the kinase domain through competing occupancy of the SH3 and SH2 domains by cognate ligands in-trans results in efficient activation of Abl (38–40). Phosphorylation of tyrosine 412 (Y^{412}) (41) in the activation helix and tyrosine 245 (Y^{245}) (42) in the kinase-SH2 linker sequence were associated with a state of high Abl kinase activity. We next investigated whether 3BP2 could modulate Abl activity in osteoblasts. 3BP2 was overexpressed in MC3T3-E1 cells, and Abl phosphorylation on residue Y^{245} was measured using a phosphospecific antibody for Abl pY^{245} as a surrogate for Abl kinase activity (42). Overexpression of 3BP2 resulted in an elevation in phosphorylated Abl protein (Figure 7C). In order to determine whether 3BP2 is required for Abl activation, primary calvarial osteoblasts from *Sh3bp2*$^{-/-}$ or wild-type mice were cultured for 14 days in osteogenic medium. Lysates from these cells were then probed with the Abl pY^{245} phosphospecific antibody. In normal cultured cells undergoing osteoblast maturation, Abl was phosphorylated, while in 3BP2-deficient cells, Abl phosphorylation was not detected (Figure 7D). These data show for what we believe is the first time that 3BP2 and Abl form a complex in vivo and that 3BP2 is required for optimal phosphorylation of Abl in osteoblasts.

3BP2 was originally identified in a phage display screen to identify Abl SH3–binding proteins (34). We verified the SH3 interaction motif present in 3BP2 as PPAYPPPPVPTPR using an overlapping peptide array derived from the entire 3BP2 sequence probed with bacterially expressed biotinylated Abl SH3 domain (data not shown). The binding affinity between the Abl SH3 domain and the 3BP2-derived peptide was 2.8 ± 0.95 μM, as measured by fluorescence polarization commensurate with other SH3 ligand–binding affinities (ref. 43 and Figure 7E).

Since occupancy of the Abl SH3 domain with peptide ligands unlocks the autoinhibited configuration of Abl and activates the enzyme (38–40, 44), we tested the capacity of the 3BP2-binding peptide to directly activate a recombinant form of Abl in vitro. A construct of Abl containing the SH3, SH2, and kinase domains was coexpressed with the YOPH phosphatase in bacteria to fully dephosphorylate and inactivate the protein as previously described (45). The recombinant protein was then purified, and Abl kinase activity in the presence of increasing concentration of the 3BP2 peptide or an irrelevant control peptide was measured using a coupled kinase assay (46). We observed that the proline-rich 3BP2 peptide potently activated Abl with a Km of 20 μM (Figure 7F). These data show that endogenous 3BP2 and Abl proteins form a complex in osteoblasts, that 3BP2 is required for optimal phosphorylation of Abl in primary osteoblasts, and that the 3BP2 Abl SH3–binding peptide can directly activate the Abl kinase in vitro.

The *Abl*$^{-/-}$ mice are osteoporotic and phenocopy some aspects of the bone abnormalities observed in the 3BP2-deficient mice (35). *Abl*$^{-/-}$ mice have reduced cortical bone thickness and trabecular bone volume as a result of dysfunctional osteoblasts. In order to determine whether the failure of *Sh3bp2*$^{-/-}$ mice to form functional osteoblasts was the result of impaired Abl activation, we introduced an activated form of Abl into *Sh3bp2*$^{-/-}$ calvarial osteoblast progenitors. A retroviral construct expressing the Abl-FKBP fusion protein was introduced into calvarial osteoblast progenitor cells by retroviral infection, selected in puromycin, and then switched to osteogenic medium containing the FKBP ligand required for dimerization and activation of the fusion protein (47). The level of Abl-FKBP tyrosine phosphorylation was confirmed in the 3BP2-deficient osteoblasts compared with wild-type and 3BP2 knockout mock-infected cells (Supplemental Figure 4). *Sh3bp2*$^{-/-}$ calvarial osteoblasts infected with the Abl-FKBP retrovirus but not mock controls regained the capacity to form mineralized nodules (Figure 7, G and H). Expression of Abl-FKBP in wild-type osteoblasts led to enhanced formation of mineralized nodules. Figure 7G shows 3 distinct phenomena: (a) ectopic expression of active Abl-FKBP rescued the defect in mineralized nodule formation observed in the 3BP2-deficient osteoblasts to wild-type levels; this result demonstrates that Abl is a functional downstream effector of 3BP2 in osteoblasts; (b) ectopic expression of active Abl-FKBP in 3BP2-sufficient cells gave rise to more mineralized nodules than was observed in the 3BP2-deficient cells, suggesting that the endogenous 3BP2 protein may promote Abl-FKBP function, presumably through proper localization and/or assembly with other important signaling molecules required for optimal osteoblast maturation; (c) ectopic expression of active Abl-FKBP in 3BP2-sufficient cells induced more mineralized nodules than was observed in the vector-alone–infected 3BP2-sufficient cells, suggesting that the Abl protein levels are limiting in the wild-type osteoblasts and that increased Abl activity can induce additional mineralized nodules. These data demonstrate that 3BP2 and Abl occupy a common signaling pathway during osteoblast maturation and that 3BP2 is normally required for Abl activation in osteoblasts.

Discussion

We have identified 3BP2 as an important regulator of bone homeostasis. 3BP2-deficient mice suffer from severe osteoporosis, with profound trabecular bone loss and reduction in bone strength as a result of combined loss-of-function within the osteoclast and osteoblast lineages.

Osteoclast defect. We have shown that osteoclasts lacking 3BP2 have an in vivo osteoclast defect. The functional loss in 3BP2-deficient osteoclasts is not a result of the failure of progenitors to undergo osteoclast lineage commitment but rather an impaired ability to form podosomes and ruffled borders required for osteoclast function. Chimeric mice derived from *Sh3bp2*$^{-/-}$ bone marrow transferred into normal irradiated hosts produced increased bone mass, demonstrating an intrinsic defect within the osteoclast

lineage lacking 3BP2. In the face of a functional osteoclast defect, we observed increased osteoclast surface to bone surface ratios in 3BP2-deficient mice, which may be a reflection of a compensatory increase in osteoclast number or a reduction in bone surface, or both. Notably, other mouse models with defective osteoclast function such as Integrin β_3– or Src-deficient mice similarly demonstrate increased osteoclast surface to bone surface ratios (3, 18). The expression levels of RANKL and its antagonist osteoprotegerin were normal in the bones of 3BP2-deficient mice, suggesting that other factors are responsible for the increase in the relative osteoclast surface observed in these mice. It is important to note that defects observed in 3BP2-deficient osteoclast appearance and function in vitro were much more severe than those observed in vivo, suggesting that a factor or combination of factors present in vivo partially rescues osteoclast function in the absence of 3BP2. In contrast to our results obtained in primary bone marrow–derived cells, 3BP2 has recently been shown to be required in the monocytic cell line RAW264.7 for osteoclast differentiation and NFATc1 induction (48). The difference in our findings may be a reflection of the differential signaling requirements characteristic for this cell line compared with primary monocytes.

Osteoblast defect. We observed that 3BP2-deficient mice are osteoporotic even in the context of an in vivo osteoclast defect, suggesting a coexisting defect within the osteoblast compartment. Although the total number of osteoblasts in *Sh3bp2*$^{-/-}$ mice as measured by histomorphometry was not diminished, we observed a significant decrease in BFR, MAR, and the mineralized surface, suggesting a functional defect of osteoblasts in vivo. Further, we observed that osteoblast progenitors from either BMSCs or calvarial-derived cells were unable to mature into functional osteoblasts in vitro or trigger a normal osteoblast transcriptional program. The reduction in osteoblast function in vitro was not a result of diminished size of the mesenchymal progenitor pool in the bone marrow but rather from a defect in osteoblast maturation.

In order to determine the existence of an intrinsic defect within the *Sh3bp2*$^{-/-}$ osteoblast compartment, we generated bone marrow chimeras in which normal bone marrow was transferred into irradiated *Sh3bp2*$^{-/-}$ recipients. These mice suffered from severe osteoporosis, demonstrating a cell autonomous osteoblast defect in vivo in the *Sh3bp2*$^{-/-}$ mice. The degree of defective bone synthesis in vivo is milder than would be predicted by the in vitro behavior of cultured osteoblasts, suggesting that the in vivo activity of osteoblasts lacking 3BP2 may be controlled developmentally or by factors missing in the in vitro culture conditions.

These data show that while 3BP2 is required for the development and function of both osteoblast and osteoclast lineages, the net reduction in bone mass observed in the *Sh3bp2*$^{-/-}$ mice argues that the normal function of 3BP2 is dominant in osteoblasts compared with osteoclasts.

3BP2 as a signaling scaffold protein connected to the cytoskeleton. We demonstrate that 3BP2 is required for the integrin-dependent activation of Src in osteoclasts. Histomorphometric analysis of *Sh3bp2*$^{-/-}$ bone showed that the percentage of trabecular bone covered by osteoclasts was elevated compared with the wild-type mice. These findings are similar to those in Src-deficient mice, which have increased numbers of TRAP-positive multinucleated osteoclasts by histomorphometry (3) but functionally impaired osteoclasts in vitro (23, 49). 3BP2-deficient osteoclasts had a reduced capacity to form podosome belts in culture or form ruffled borders in vivo. Similarly, Src-deficient osteoclasts fail to organize their actin cytoskeleton or form ruffled borders and are impaired in their capacity to resorb bone (50). Expression of an activated form of Src rescues the formation of large osteoclasts with resorbing capacity in vitro, demonstrating the requirement of 3BP2 for Src necessary to stimulate organized polymerized actin structures in osteoclasts. The downstream effector Src proteins, Syk and Vav proteins, are poorly phosphorylated in the absence of 3BP2. It is important to note that the in vivo phenotype of the *Sh3bp2*$^{-/-}$ osteoclast defect is less severe than what is observed in the *Src*$^{-/-}$ mice. We attribute this difference to residual Src and Syk activity observed in the absence of 3BP2 (Figure 5). Therefore, complete loss-of-function of 3BP2 results in a partial, hypomorphic Src defect, which is reflected in a less severe osteoclast defect compared with the complete Src knockout phenotype. The phenotype observed in the *Sh3bp2*$^{-/-}$ osteoclasts closely phenocopies mice lacking Syk or the Syk substrates Slp76 and BLNK, which produce normally differentiated osteoclasts that are functionally defective (4, 51), suggesting that 3BP2 is part of a common pathway involving Src, Syk, and Slp76/BLNK.

The formation of differentiated osteoclasts from macrophage progenitors requires integration of signals from c-Fms, DAP12/FcRγ, and $\alpha_v\beta_3$ integrin cell surface receptors (52–55). How 3BP2 links these cell surface receptors to Src activation and phosphorylation of Syk and Vav proteins remains unresolved, but clearly 3BP2 is essential for this signal propagation in osteoclasts. 3BP2 may function as an anchoring protein to assemble these signaling proteins, possibly in a processive manner, to coordinate and optimize signals emanating from these receptors.

3BP2 as an Abl activator SH3 ligand. In order to elucidate the mechanism by which 3BP2 regulates osteoblast function, we examined the role of the 3BP2 interacting protein, the Abl tyrosine kinase, a protein known to be essential for normal osteoblast function (25). Abl-deficient mice are osteopenic with a reduced BFR resulting from an intrinsic osteoblast maturation defect. The similarity of the osteoblast phenotype observed in both Abl- and 3BP2-deficient mice suggested that they may be part of a common signaling pathway. We showed that both 3BP2 and Abl are coordinately expressed during osteoblast maturation and show that they form an endogenous complex in vivo. We have demonstrated that Abl is tyrosine phosphorylated on tyrosine-245 in primary osteoblasts but fails to become phosphorylated on this residue at high levels in the absence of 3BP2. 3BP2 is a unique Abl SH3–binding protein, as other proteins of its class, including 3BP-1 (2), Cbl (38), Dok-R (40), ST5 (44), and Abi-1 (56), have not been shown to be required for Abl activation in vivo. Tyrosine-245 is a regulatory residue in the SH2-kinase linker sequence, which is part of the SH3-binding surface when Abl is in its autoinhibited state (37). Occupancy of the liberated Abl SH3 domain by a proline-rich ligand in-trans reinforces the open active state of Abl. We confirmed that Abl binds directly via its SH3 domain to a specific proline-rich sequence in 3BP2 with high affinity and show that the 3BP2-derived binding peptide potently activates the Abl kinase in vitro. These data demonstrate that 3BP2 is a natural SH3 ligand for Abl in vivo and is part of a regulatory protein complex required for optimal activation of Abl in developing osteoblasts.

In order to demonstrate that Abl operates downstream of 3BP2, we expressed a constitutively activated Abl construct in the *Sh3bp2*$^{-/-}$ calvarial-derived osteoblast progenitors and were able to rescue their maturation defect. These data conclusively show that Abl is positively regulated by 3BP2 in developing osteoblasts and that

the failure to activate Abl normally in the 3BP2-deficient mice likely accounts for the osteopenic phenotype observed in these mice. Exposure to Abl inhibitors leads to increased trabecular bone mass in chronic myelogenous leukemia (CML) patients (57). This is an unexpected result, given the observation that Abl-deficient mice are osteoporotic as a result of an osteoblast defect (35). The apparent discrepancy is likely due to the spectrum of inhibitory activities of Imatinib against CSF-1 and PDGF receptors. Inhibition of CSF1-R results in osteoclast impairment, while inhibition of PDGFR promotes Abl-independent osteoblastogenesis (57, 58). Thus, Imatinib has complex effects on both osteoclast and osteoblast function. Future studies will be needed to identify the upstream receptors through which Abl is coupled by 3BP2 and the physiologic downstream Abl substrates required for osteoblast maturation.

In summary, we have identified 3BP2 as a unique adapter protein that controls both osteoblast and osteoclast lineages. We have uncovered a role for 3BP2 in regulating osteoblast maturation, which is dominant over its role in osteoclasts under physiologic conditions. 3BP2 is required for the proper coordination of synthesis and resorption necessary to maintain bone homeostasis through the engagement and activation of the related nonreceptor tyrosine kinases Abl and Src in osteoblasts and osteoclasts, respectively.

Methods

Mice. Derivation of *Sh3bp2*$^{-/-}$ mice has been previously described (9). The *Sh3bp2*$^{-/-}$ mice have been crossed onto the C57BL/6 background for 10 generations. 10^6 bone marrow cells from B6.SJL (Ly5.1) mice (Taconic) were injected into the tail veins of either 8-week-old irradiated (9 Gy) C57BL/6 (Ly5.2) control or *Sh3bp2*$^{-/-}$ (Ly5.2) recipient mice. Chimerism representing 85% donor cells was confirmed by flow cytometry and trabecular bone volume measured by μCT 8 weeks after transfer. Reciprocal chimeras were made using *Sh3bp2*$^{-/-}$ as donors into irradiated B6.SJL recipient mice. All animal studies were approved by the Animal Research Council at University Health Network, Toronto, Ontario.

Microcomputed tomography. μCT (SkyScan) was performed on femurs from 12-week-old wild-type or *Sh3bp2*$^{-/-}$ male mice. Analysis of trabecular bone was performed over 2 mm in length, 0.4 mm below the distal growth plate. Analysis of cortical bone was performed on a region of 1 mm in length in the midshaft. Each image was reconstructed from 200 11.7-μm slices 0.4 mm below the growth plate, and trabecular morphometric parameters were determined according to standard protocols (59). A fixed density threshold was determined using a pair of calibration phantoms (SkyScan).

Histomorphometry. For dynamic histomorphometry, calcein green was injected on day 1 followed by xylenol orange on day 7 and mice sacrificed 2 days after the second calcein injection. Undecalcified femora sections were embedded in methyl methacrylate. In vivo osteoblast and osteoclast parameters were generated from paraffin sections of decalcified femurs or tibias stained with H&E or TRAP, and images were analyzed using Bio-Quant software. All measurements were taken in an area of 600,000–1,200,000 SQ microns located 0.4 mm below the growth plates.

Bone mechanical testing. For bone mechanical testing, excised vertebral bodies were dissected from thawed spine and their processes removed for subsequent compression testing. Coronal and transversal images of the individual vertebrae were obtained using a stereoscope (Leica M3Z) connected to a digital camera. Images were analyzed using image analysis software (ImageJ 1.28u; NIH), which generated data on vertebral body area (*A* in mm^2) and length (*l* in mm). Vertebrae were then subjected to uniaxial compression at 0.5 mm/min with a 100-N load cell on an Instron 4465 material testing system (Instron) as described (60).

Western blotting, immunoprecipitation, immunofluorescence, and pull-down assays. Cells were lysed with HNMETG buffer (50 mM Hepes [pH 7.5], 150 mM NaCl, 1.5 mM $MgCl_2$, 1.0 mM EGTA, 1.0% Triton X-100, 10% glycerol) or RIPA buffer (50 mM Tris [pH 7.5], 150 mM NaCl, 1% NP40, 0.1% SDS, 0.25% sodium deoxycholate, 1 mM EDTA) supplemented with 10 mM NaF, 2 mM Na_3VO_4, and complete protease inhibitor tablets (Roche). Lysates were cleared by centrifugation for 10 minutes at 10,000 *g* and 4°C. Immunoprecipitation was performed with indicated antibodies, and the products collected on protein A or G sepharose beads, washed 3 times with HNMETG buffer containing 0.1% Triton X-100, eluted into SDS sample buffer, and resolved by SDS-PAGE. Gels were transferred to PVDF membranes (Immobilon; Millipore). For phosphotyrosine blotting, membranes were blocked in 2% BSA in PBST (PBS + 0.05% Tween-20). For other antibodies, the blocking buffer used was 5% nonfat dried milk (Carnation) in PBST. Membranes were developed using ECL or ECL plus (Amersham). RacGTP levels were measured using a PAK GST-PBD pull-down assay. Recombinant PAK GST-PBD immobilized on beads was used to precipitate RacGTP from lysates. Complexes were resolved by SDS-PAGE and immunoblotted with anti-Rac antibody. For actin immunofluorescence on glass, cells were fixed in 3.7% paraformaldehyde, permeabilized with 0.2% Triton X-100 in PBS, then blocked in 3% BSA in PBS. Cells were stained with Texas red phalloidin and then with DAPI. The percentage of the perimeter with podosome belts was performed using ImageJ software (NIH). The actin ring length was determined for each cell manually and then divided by the cell perimeter. For Runx2 immunofluorescence, calvarial osteoblasts were fixed in 3.7% PFA, permeabilized with 0.2% Triton X-100 in PBS, blocked in 2% BSA in PBS, and then incubated with a mouse anti-Runx2 antibody. Goat anti-mouse Alexa Fluor 594 antibody was used as a secondary antibody, and nuclei were stained by DAPI (Invitrogen).

TEM. Excised vertebral bodies from 4-week-old wild-type and *Sh3bp2*$^{-/-}$ mice were fixed in 2% glutaraldehyde in 0.1 M sodium cacodylate buffer, demineralized in 8% formic acid, post-fixed in 1% osmium tetroxide in cacodylate buffer, dehydrated in a graded ethanol series followed by propylene oxide, and embedded in Quetol Spurr resin. Sections 100-nm thick were cut on an RMC MT6000 ultramicrotome, stained with uranyl acetate and lead citrate, and viewed in an FEI Tecnai 20 TEM.

Osteoclast isolation and analysis. Bone marrow cells were isolated from mice and treated with ACK buffer to remove red blood cells. Cells were plated at 10^6 cells/ml in α-MEM containing 10% FBS, 50 U/l penicillin and 50 μg/l streptomycin, and 10 ng/ml CSF-1 for 2 days. The resulting BMMs were suspended in the same medium with the addition of 40 ng/ml RANKL. Cells were plated at 5×10^5 cells/cm^2 in 12-well plates. Medium was changed after 3 days of culture. At day 5 after the addition of RANKL, cells were stained for Tartrate Resistant Acid Phosphatase (–386A; Sigma-Aldrich).

Dentine resorption assays. 2×10^5 BMMs were plated on dentine discs with RANKL in 96-well plates and cultured for 14 days, with the medium replaced every 2 days. Osteoclasts were fixed in 3.7% paraformaldehyde, TRAP stained, and counted. Discs were incubated with 0.25 M ammonium hydroxide and mechanically agitated gently for 1 hour. The discs were stained with 0.1% toluidine blue in 0.5% sodium tetraborate for 5 minutes, washed with water, and air dried before photographs were taken. Raw264.7 cells were differentiated into osteoclasts by plating cells at 10,000 cells/cm^2 in the presence of 10 ng/ml CSF-1 and 40 ng/ml RANKL for 5 days.

Osteoblast cultures. Long bone osteoblasts from 8-week-old mice or neonatal calvarial-derived osteoblasts were harvested and cultured as described (61). MC3T3-E1 (ATCC) was cultured in α-MEM (Gibco; Invitrogen) containing 10% FBS (Hyclone). Osteoblast differentiation was induced by culturing cells in osteogenic medium (α-MEM containing 10% FBS, 100 μg/ml ascorbic acid, 10 mM β-glycerophosphate, 10^{-8} M dexamethasone) for 21 days. ALP staining and quantification were performed as described

(61). Detection of collagen matrix using picric acid and mineralization as measured by alizarin red and von Kossa staining of osteoblast cultures were performed as described (61).

FACS analysis of skeletal stem cells. Bone marrow cells were flushed from the femurs of 12-week-old wild-type or *Sh3bp2*$^{-/-}$ mice. Cell aliquots were incubated for 20 minutes at 4°C with anti-mouse PE Sca-1–, FITC-CD29, peridinin chlorophyll protein–CD45– (PerCP-CD45), and allophycocyanin-CD11b–conjugated (APC-CD11b) antibodies (BioLegend). FACS acquisition was performed and analyzed with a FACS DIVE software version 6.1.3 (BD Biosciences).

CFU-F and CFU-Ob assays. Nucleated bone marrow cells were seeded at a density of 0.5×10^6 cells/well in 6-well plates and cultured 14 days in Mesencult MSC Basal Medium (StemCell Technologies). Colonies containing 50 or more cells were counted. CFU-Obs were induced by culturing CFU-Fs in osteogenic medium for 28 days.

Quantitative RT-PCR assay. Quantitative RT-PCR was performed on an ABI 7900 HT system using the TaqMan Gene Expression assays (Applied Biosystems) for *Runx2* (Mm00501580_m1), *Osterix* (Mm00504574_m1), *Osteocalcin* (Mm03413926_mH), *GAPDH* (4352339_E), *Nfatc1* (Mm00479441_m1), DC-STAMP (Mm01219007_m1), and *Atp6v0d2* (Mm00656638_m1). The primers for *Tnfsf11* and *Tnfsf11b* were as described in ref. 62.

Integrin stimulation. Preosteoclasts were incubated with CSF-1 and RANKL for 3 days, starved in medium containing 0.5% FBS for 4 hours, then lifted with PBS containing 10 mM EDTA. Preosteoclasts were plated either on osteopontin- (10 μg/ml) or poly-L-lysine–coated (0.01%, Sigma-Aldrich) dishes for 30 minutes. Cells were lysed in RIPA buffer as described.

Construction and expression of 3BP2 and Y527F Src retroviral vectors. pMIG 3BP2 was created by cloning mouse *Sh3bp2* cDNA into pMIG using the EcoRI restriction site (Addgene). pMIG Y527F Src was generated by amplifying the sequence encoding Y527F Src in pLNCX chick Src Y527F (Addgene), introducing EcoRI restriction sites, followed by cloning into the corresponding site in pMIG. Retroviral supernatants were generated using the PlatE packaging cell line (Cell Biolabs). BMMs were isolated and plated at 5×10^5 cells in bacterial Petri dishes. On the following day, cells were inoculated with retroviruses at an MOI of 10. Forty-eight hours after infection, percentage of infected cells was verified by GFP expression using fluorescence microscopy.

Construction and expression of Abl-FKBP retroviral vectors. pMx-Abl-FKBP was derived from pMSCVhyg-Abl-FKBP (47), introducing a BamHI and a NotI restriction site. The PCR product was cloned into the BamHI and NotI sites of pMx-puro. Retroviral supernatants were generated using the PlatE packaging cell line. Osteoblasts were infected, selected in puromycin, and then cultured in osteogenic medium containing 50 nM AP20187 (ARIAD) for 28 days. AP20187 was replenished every 3 days.

CTX-I and PINP ELISA. ELISA measurement of serum N-terminal PINP (IDS) and carboxyterminal cross-linking telopeptide of type I collagen (CTX-I) (IDS) were performed on 12-week-old mice according to the manufacturer's instruction.

Fluorescence polarization and Abl kinase assay. Fluorescence polarization of FITC-conjugated 3BP2 peptide KLDALTYPPAYPPPPVPVPRK was measured in the presence of increasing concentrations of recombinant Abl SH3 domain protein. Two other 3BP2-derived peptides, RVEPGLRVPATPRRMS and RGSRSPHDGLER, were used as controls. The activity of recombinant Abl SH3SH2-kinase protein cassette in the presence of increasing concentrations of the 3BP2-derived Abl SH3–binding peptide was measured in a continuous kinase assay (45). Recombinant, Abl protein was coexpressed with the YOPH phosphatase in bacteria and purified as described (45). Aprotinin peptide was used as a negative control. EAIYAAPFAKKK peptide was used as the Abl substrate. These data are representative of 4 independent experiments.

Statistics. Data are presented as mean ± SEM. Statistical significance was determined by 2-tailed Student's *t* test. $P < 0.05$ was considered statistically significant.

Acknowledgments

The authors would like to thank J. Wang (UCSD) for the Abl-FKBP construct and F. Sicheri for advice on fluorescence polarization. N. Levaot was supported by the Arthritis Centre for Excellence fellowship, University of Toronto. This work was supported by a grant from the Terry Fox Research Institute and the Canadian Cancer Society Research Institute. This research was funded in part by the Ontario Ministry of Health and Long Term Care. The views expressed do not necessarily reflect those of the Ontario Ministry of Health and Long Term Care.

Received for publication November 18, 2010, and accepted in revised form June 1, 2011.

Address correspondence to: Robert Rottapel, Toronto Medical Discovery Tower, MaRS East Tower, 8-703, 101 College Street, Toronto, Ontario M5G 1L7, Canada. Phone: 416.581.7852; Fax: 416.595.5719; E-mail: rottapel@uhnres.utoronto.ca.

1. Deckert M, Rottapel R. The adapter 3BP2: how it plugs into leukocyte signaling. *Adv Exp Med Biol*. 2006;584:107–114.
2. Cicchetti P, Mayer BJ, Thiel G, Baltimore D. Identification of a protein that binds to the SH3 region of Abl and is similar to Bcr and GAP-rho. *Science*. 1992; 257(5071):803–806.
3. Soriano P, Montgomery C, Geske R, Bradley A. Targeted disruption of the c-src proto-oncogene leads to osteopetrosis in mice. *Cell*. 1991;64(4):693–702.
4. Zou W, et al. Syk, c-Src, the alphavbeta3 integrin, and ITAM immunoreceptors, in concert, regulate osteoclastic bone resorption. *J Cell Biol*. 2007; 176(6):877–888.
5. Faccio R, et al. Vav3 regulates osteoclast function and bone mass. *Nat Med*. 2005;11(3):284–290.
6. Jones WA, Gerrie J, Pritchard J. Cherubism––familial fibrous dysplasia of the jaws. *J Bone Joint Surg Br*. 1950;32-B(3):334–347.
7. Ueki Y, et al. Mutations in the gene encoding c-Abl-binding protein SH3BP2 cause cherubism. *Nat Genet*. 2001;28(2):125–126.
8. Ueki Y, et al. Increased myeloid cell responses to M-CSF and RANKL cause bone loss and inflammation in SH3BP2 "cherubism" mice. *Cell*. 2007; 128(1):71–83.
9. Chen G, et al. The 3BP2 adapter protein is required for optimal B-cell activation and thymus-independent type 2 humoral response. *Mol Cell Biol*. 2007;27(8):3109–3122.
10. Lowe C, Yoneda T, Boyce BF, Chen H, Mundy GR, Soriano P. Osteopetrosis in Src-deficient mice is due to an autonomous defect of osteoclasts. *Proc Natl Acad Sci U S A*. 1993;90(10):4485–4489.
11. Wang ZQ, Ovitt C, Grigoriadis AE, Mohle-Steinlein U, Ruther U, Wagner EF. Bone and haematopoietic defects in mice lacking c-fos. *Nature*. 1992; 360(6406):741–745.
12. Dumas A, Brigitte M, Moreau MF, Chretien F, Basle MF, Chappard D. Bone mass and microarchitecture of irradiated and bone marrow-transplanted mice: influences of the donor strain. *Osteoporos Int*. 2009; 20(3):435–443.
13. Mao D, Epple H, Uthgenannt B, Novack DV, Faccio R. PLCgamma2 regulates osteoclastogenesis via its interaction with ITAM proteins and GAB2. *J Clin Invest*. 2006;116(11):2869–2879.
14. Shukla U, Hatani T, Nakashima K, Ogi K, Sada K. Tyrosine phosphorylation of 3BP2 regulates B cell receptor-mediated activation of NFAT. *J Biol Chem*. 2009;284(49):33719–33728.
15. Yagi M, et al. DC-STAMP is essential for cell-cell fusion in osteoclasts and foreign body giant cells. *J Exp Med*. 2005;202(3):345–351.
16. Lee SH, et al. v-ATPase V0 subunit d2-deficient mice exhibit impaired osteoclast fusion and increased bone formation. *Nat Med*. 2006;12(12):1403–1409.
17. Kim K, Lee SH, Ha Kim J, Choi Y, Kim N. NFATc1 induces osteoclast fusion via up-regulation of Atp6v0d2 and the dendritic cell-specific transmembrane protein (DC-STAMP). *Mol Endocrinol*. 2008; 22(1):176–185.
18. McHugh KP, et al. Mice lacking beta3 integrins are osteosclerotic because of dysfunctional osteoclasts. *J Clin Invest*. 2000;105(4):433–440.
19. Nakamura I, et al. Role of alpha(v)beta(3) integrin in osteoclast migration and formation of the sealing zone. *J Cell Sci*. 1999;112(pt 22):3985–3993.
20. Sato M, et al. Structure-activity studies of the s-echistatin inhibition of bone resorption. *J Bone Miner Res*. 1994;9(9):1441–1449.
21. Yamamoto M, et al. The integrin ligand echistatin

prevents bone loss in ovariectomized mice and rats. *Endocrinology*. 1998;139(3):1411–1419.
22. Crippes BA, et al. Antibody to beta3 integrin inhibits osteoclast-mediated bone resorption in the thyroparathyroidectomized rat. *Endocrinology*. 1996; 137(3):918–924.
23. Sanjay A, et al. Cbl associates with Pyk2 and Src to regulate Src kinase activity, alpha(v)beta(3) integrin-mediated signaling, cell adhesion, and osteoclast motility. *J Cell Biol*. 2001;152(1):181–195.
24. Miyazaki T, Sanjay A, Neff L, Tanaka S, Horne WC, Baron R. Src kinase activity is essential for osteoclast function. *J Biol Chem*. 2004;279(17):17660–17666.
25. Arias-Salgado EG, Lizano S, Sarkar S, Brugge JS, Ginsberg MH, Shattil SJ. Src kinase activation by direct interaction with the integrin beta cytoplasmic domain. *Proc Natl Acad Sci U S A*. 2003; 100(23):13298–13302.
26. Maeno K, et al. Adaptor protein 3BP2 is a potential ligand of Src homology 2 and 3 domains of Lyn protein-tyrosine kinase. *J Biol Chem*. 2003; 278(27):24912–24920.
27. Foucault I, Le Bras S, Charvet C, Moon C, Altman A, Deckert M. The adaptor protein 3BP2 associates with VAV guanine nucleotide exchange factors to regulate NFAT activation by the B-cell antigen receptor. *Blood*. 2005;105(3):1106–1113.
28. Woodside DG, et al. Activation of Syk protein tyrosine kinase through interaction with integrin beta cytoplasmic domains. *Curr Biol*. 2001;11(22):1799–1804.
29. Deckert M, Tartare-Deckert S, Hernandez J, Rottapel R, Altman A. Adaptor function for the Syk kinases-interacting protein 3BP2 in IL-2 gene activation. *Immunity*. 1998;9(5):595–605.
30. Zakaria S, et al. Differential regulation of TCR-mediated gene transcription by Vav family members. *J Exp Med*. 2004;199(3):429–434.
31. Wu X, et al. Inhibition of Sca-1-positive skeletal stem cell recruitment by alendronate blunts the anabolic effects of parathyroid hormone on bone remodeling. *Cell Stem Cell*. 2010;7(5):571–580.
32. Xu Y, Malladi P, Zhou D, Longaker MT. Molecular and cellular characterization of mouse calvarial osteoblasts derived from neural crest and paraxial mesoderm. *Plast Reconstr Surg*. 2007;120(7):1783–1795.
33. Ducy P, Zhang R, Geoffroy V, Ridall AL, Karsenty G. Osf2/Cbfa1: a transcriptional activator of osteoblast differentiation. *Cell*. 1997;89(5):747–754.
34. Ren R, Mayer BJ, Cicchetti P, Baltimore D. Identification of a ten-amino acid proline-rich SH3 binding site. *Science*. 1993;259(5098):1157–1161.
35. Li B, et al. Mice deficient in Abl are osteoporotic and have defects in osteoblast maturation. *Nat Genet*. 2000;24(3):304–308.
36. Quarles LD, Yohay DA, Lever LW, Caton R, Wenstrup RJ. Distinct proliferative and differentiated stages of murine MC3T3-E1 cells in culture: an in vitro model of osteoblast development. *J Bone Miner Res*. 1992;7(6):683–692.
37. Nagar B, et al. Structural basis for the autoinhibition of c-Abl tyrosine kinase. *Cell*. 2003;112(6):859–871.
38. Miyoshi-Akiyama T, Aleman LM, Smith JM, Adler CE, Mayer BJ. Regulation of Cbl phosphorylation by the Abl tyrosine kinase and the Nck SH2/SH3 adaptor. *Oncogene*. 2001;20(30):4058–4069.
39. Barila D, et al. A nuclear tyrosine phosphorylation circuit: c-Jun as an activator and substrate of c-Abl and JNK. *EMBO J*. 2000;19(2):273–281.
40. Master Z, et al. Dok-R binds c-Abl and regulates Abl kinase activity and mediates cytoskeletal reorganization. *J Biol Chem*. 2003;278(32):30170–30179.
41. Tanis KQ, Veach D, Duewel HS, Bornmann WG, Koleske AJ. Two distinct phosphorylation pathways have additive effects on Abl family kinase activation. *Mol Cell Biol*. 2003;23(11):3884–3896.
42. Brasher BB, Van Etten RA. c-Abl has high intrinsic tyrosine kinase activity that is stimulated by mutation of the Src homology 3 domain and by autophosphorylation at two distinct regulatory tyrosines. *J Biol Chem*. 2000;275(45):35631–35637.
43. Mayer BJ. SH3 domains: complexity in moderation. *J Cell Sci*. 2001;114(pt 7):1253–1263.
44. Majidi M, Hubbs AE, Lichy JH. Activation of extracellular signal-regulated kinase 2 by a novel Abl-binding protein, ST5. *J Biol Chem*. 1998; 273(26):16608–16614.
45. Seeliger MA, et al. High yield bacterial expression of active c-Abl and c-Src tyrosine kinases. *Protein Sci*. 2005;14(12):3135–3139.
46. Barker SC, Kassel DB, Weigl D, Huang X, Luther MA, Knight WB. Characterization of pp60c-src tyrosine kinase activities using a continuous assay: autoactivation of the enzyme is an intermolecular autophosphorylation process. *Biochemistry*. 1995; 34(45):14843–14851.
47. Jin H, Wang JY. Abl tyrosine kinase promotes dorsal ruffles but restrains lamellipodia extension during cell spreading on fibronectin. *Mol Biol Cell*. 2007; 18(10):4143–4154.
48. GuezGuez A, et al. 3BP2 Adapter protein is required for receptor activator of NFkappaB ligand (RANKL)-induced osteoclast differentiation of RAW264.7 cells. *J Biol Chem*. 2010;285(27):20952–20963.
49. Horne WC, Neff L, Chatterjee D, Lomri A, Levy JB, Baron R. Osteoclasts express high levels of pp60c-src in association with intracellular membranes. *J Cell Biol*. 1992;119(4):1003–1013.
50. Boyce BF, Yoneda T, Lowe C, Soriano P, Mundy GR. Requirement of pp60c-src expression for osteoclasts to form ruffled borders and resorb bone in mice. *J Clin Invest*. 1992;90(4):1622–1627.
51. Reeve JL, Zou W, Liu Y, Maltzman JS, Ross FP, Teitelbaum SL. SLP-76 couples Syk to the osteoclast cytoskeleton. *J Immunol*. 2009;183(3):1804–1812.
52. Mocsai A, et al. The immunomodulatory adapter proteins DAP12 and Fc receptor gamma-chain (FcRgamma) regulate development of functional osteoclasts through the Syk tyrosine kinase. *Proc Natl Acad Sci U S A*. 2004;101(16):6158–6163.
53. Zou W, Reeve JL, Liu Y, Teitelbaum SL, Ross FP. DAP12 couples c-Fms activation to the osteoclast cytoskeleton by recruitment of Syk. *Mol Cell*. 2008; 31(3):422–431.
54. Lanier LL, Corliss BC, Wu J, Leong C, Phillips JH. Immunoreceptor DAP12 bearing a tyrosine-based activation motif is involved in activating NK cells. *Nature*. 1998;391(6668):703–707.
55. Insogna KL, et al. Colony-stimulating factor-1 induces cytoskeletal reorganization and c-src-dependent tyrosine phosphorylation of selected cellular proteins in rodent osteoclasts. *J Clin Invest*. 1997; 100(10):2476–2485.
56. Shi Y, Alin K, Goff SP. Abl-interactor-1, a novel SH3 protein binding to the carboxy-terminal portion of the Abl protein, suppresses v-abl transforming activity. *Genes Dev*. 1995;9(21):2583–2597.
57. Fitter S, et al. Long-term imatinib therapy promotes bone formation in CML patients. *Blood*. 2008;111(5):2538–2547.
58. Dewar AL, et al. Imatinib as a potential antiresorptive therapy for bone disease. *Blood*. 2006; 107(11):4334–4337.
59. Parfitt AM. Trabecular bone architecture in the pathogenesis and prevention of fracture. *Am J Med*. 1987;82(1B):68–72.
60. Mousny M, et al. The genetic influence on bone susceptibility to fluoride. *Bone*. 2006;39(6):1283–1289.
61. Ralston S, Helfrich MH. *Bone Research Protocols*. Totowa, New Jersey, USA: Humana Press; 2003.
62. Cao J, Venton L, Sakata T, Halloran BP. Expression of RANKL and OPG correlates with age-related bone loss in male C57BL/6 mice. *J Bone Miner Res*. 2003;18(2):270–277.